Synthesis, Crystal Structures, and Magnetic Properties of New 12L-Perovskites $Ba_4LnRu_3O_{12}$ (Ln = Lanthanides)

Yuki Shimoda,* Yoshihiro Doi, and Yukio Hinatsu

Division of Chemistry, Graduate School of Science, Hokkaido University, Sapporo 060-0810, Japan

Kenji Ohoyama

Institute for Materials Research, Tohoku University, Sendai 980-8577, Japan

Received March 11, 2008. Revised Manuscript Received May 9, 2008

Synthesis, crystal structures, and magnetic properties of new quaternary oxides $Ba_4LnRu_3O_{12}$ (Ln = lanthanides) were investigated. From the powder X-ray and neutron diffraction measurements, it is found that they adopt the 12L-perovskite-type structures consisting of Ru_3O_{12} trimers and LnO_6 octahedra. The $Ba_4LnRu_3O_{12}$ for Ln = Tb−Lu have a hexagonal unit cell with the space group $R\bar{3}m$, while those for Ln = La−Nd, Sm−Gd have a monoclinically distorted cell with $C2/m$. Only for Ln = Ce, Pr, and Tb compounds, the Ln ions are in the tetravalent state. The magnetic properties of these three compounds were investigated. For $Ba_4CeRu_3O_{12}$, no magnetic transition was observed down to 0.5 K. The $Ba_4PrRu_3O_{12}$ and $Ba_4TbRu_3O_{12}$ show an antiferromagnetic transition at 2.4 and 24 K, respectively. The magnetic structure for $Ba_4TbRu_3O_{12}$ was determined by powder neutron diffraction measurements at low temperatures, which indicates the long-range antiferromagnetic ordering.

Introduction

Perovskite and perovskite-like oxides containing ruthenium ions often exhibit interesting magnetic and electrical properties.[1,2] The crystal structure of the perovskite oxide ABO_3 can be described as a framework of corner-shared BO_6 octahedra, which contains A cations at 12-coordinate sites. Since the B cations generally determine the physical properties of perovskites, the combination of different kinds of B cations (B′ and B″ cations) may bring about attractive properties.

When the size and/or charge of the B′ and B″ cations are sufficiently different, $AB'_{0.5}B''_{0.5}O_3$ can order, doubling the formula unit. The structural chemistry and magnetic properties of the double perovskites A_2LnRuO_6 (A = Sr, Ba; Ln = lanthanides) have been studied in detail.[3–9] In them, the Ln and Ru ions are regularly ordered over the six-coordinate B sites. These compounds show an antiferromagnetic transition at low temperatures. The Néel temperature changes widely from 26 to 117 K. This feature is affected by the properties of Ln ions. In addition, a complicated temperature dependence of the magnetic susceptibilities is observed below the transition temperatures, reflecting the magnetic interaction between Ru and Ln ions.

In addition, when the ratio of B site cations (B′ and B″) is changed, a great variety of alignments of B′ and B″ may result. Structures of perovskite compounds can be regarded as the stacking of close-packed AO_3 layers and the filling of subsequent octahedral sites by B site ions. The difference in the stacking sequence changes the way of linkage of BO_6 octahedra: the corner-sharing BO_6 in the cubic perovskite (3L: three-layer) with *abc*... sequence, the face-sharing BO_6 in 2L-perovskite (2L: two-layer) with *ab*... sequence, and mixed linkages between the corner- and face-sharing in various intergrowth structures.[10]

Recently, the 6L-perovskites $Ba_3LnRu_2O_9$ (the stacking sequence: *abacbc*...) have been investigated.[11–17] In this structure, two RuO_6 octahedra are connected by face-sharing and form a Ru_2O_9 dimer. These dimers and LnO_6 octahedra are placed alternately; thus, a 6-layer (6L) structure is generated. These compounds also show magnetic ordering

* To whom correspondence should be addressed.

(1) Callanghan, A.; Moeller, C. W.; Ward, R. *Inorg. Chem.* **1965**, *5*, 1572–1576.
(2) Maeno, Y.; Hashimoto, H.; Yoshida, K.; Nishizaki, S.; Fujita, T.; Bednorz, J. G.; Lichtenberg, F. *Nature* **1994**, *372*, 532–534.
(3) Gibb, T. C.; Greatrex, R. *J. Solid State Chem.* **1980**, *34*, 279–288.
(4) Battle, P. D.; Jones, C. W.; Studer, F. *J. Solid State Chem.* **1991**, *90*, 302–312.
(5) Doi, Y.; Hinatsu, Y. *J. Phys.: Condens. Matter* **1999**, *11*, 4813–4820.
(6) Izumiyama, Y.; Doi, Y.; Wakeshima, M.; Hinatsu, Y.; Oikawa, K.; Shimojo, Y.; Morii, Y. *J. Mater. Chem.* **2000**, *10*, 2364–2367.
(7) Izumiyama, Y.; Doi, Y.; Wakeshima, M.; Hinatsu, Y.; Shimojo, Y.; Morii, Y. *J. Phys.: Condens. Matter.* **2001**, *13*, 1303–1313.
(8) Izumiyama, Y.; Doi, Y.; Wakeshima, M.; Hinatsu, Y.; Nakamura, A.; Ishii, Y. *J. Solid State Chem.* **2002**, *169*, 125–130.
(9) Doi, Y.; Hinatsu, Y.; Nakamura, A.; Ishii, Y.; Morii, Y. *J. Mater. Chem.* **2003**, *13*, 1758–1763.
(10) Longo, J. M.; Kafalas, J. A. *J. Solid State Chem.* **1969**, *1*, 103–108.
(11) Thumm, I.; Treiber, U.; Kemmler-Sack, S. *Z. Anorg. Allg. Chem.* **1981**, *477*, 161–166.
(12) Treiber, U.; Kemmler-Sack, S.; Ehmann, A.; Achaller, H. U.; Dürrschmidt, E.; Thumm, I.; Bader, H. *Z. Anorg. Allg. Chem.* **1981**, *481*, 143–152.
(13) Rath, M.; Müller-Buschbaum, H. *J. Alloys Compd.* **1994**, *210*, 119–123.
(14) Doi, Y.; Hinatsu, Y.; Shimojo, Y.; Ishii, Y. *J. Solid State Chem.* **2001**, *161*, 113–120.
(15) Doi, Y.; Wakeshima, M.; Hinatsu, Y.; Tobo, A.; Ohoyama, K.; Yamaguchi, Y. *J. Mater. Chem.* **2001**, *11*, 3135–3140.
(16) Doi, Y.; Matsuhira, K.; Hinatsu, Y. *J. Solid State Chem.* **2002**, *165*, 317–323.
(17) Doi, Y.; Hinatsu, Y. *J. Mater. Chem.* **2002**, *12*, 1792–1795.

10.1021/cm800708g CCC: $40.75
Published on Web 06/12/2008

at low temperatures. The predicted magnetic exchange pathways are Ru−O−Ru in the Ru_2O_9 dimer and Ru−O−Ln. Moreover, these compounds show unusual magnetic behavior even at room temperature since strong magnetic interactions between Ru ions exist because of the short Ru−Ru bond length.

Now, we focus our attention on new compounds $Ba_4LnRu_3O_{12}$ in which the ratio of Ln:Ru is 1:3. In the $Ba_4LnRu_3O_{12}$, three RuO_6 octahedra are face-shared, forming a Ru_3O_{12} trimer, and we may find peculiar magnetic behavior due to new alignment of the Ln and Ru ions. In the $Ba_3LnRu_2O_9$, the ground state of the total spin of the isolated Ru_2O_9 dimer may be zero, i.e., $S_{total} = S_1 + S_2 = 0$, for the case that the antiferromagnetic coupling exists between the Ru ions. On the other hand, when we consider $Ba_4LnRu_3O_{12}$ compounds, the total magnetic moment of the Ru_3O_{12} trimer does not disappear as far as three Ru ions are equivalent in the trimer. In such a case, the magnetic interaction between Ru_3O_{12} trimers and Ln ions will be important, and unique magnetic behavior reflecting this structure should be expected.

In this work, we took on the challenge of preparing new perovskite compounds $Ba_4LnRu_3O_{12}$ and investigated their magnetic properties.

Experimental Section

Synthesis. Polycrystalline samples (0.3 g) of $Ba_4LnRu_3O_{12}$ (Ln = La−Nd, Sm−Lu) were prepared by the standard solid-state reaction. BaO, BaO_2, Ru, RuO_2, and Ln_2O_3 (or CeO_2, Pr_6O_{11}, Tb_4O_7) were used as starting materials. For La_2O_3 and Nd_2O_3, they absorb moisture in air and easily form lanthanide hydroxides $Ln(OH)_3$. Therefore, we preheated these compounds at 900 °C for 12 h to decompose them into Ln_2O_3 before use. For better reactivity, the thermally decomposed products (500 °C for 4 h) of lanthanide nitrates (Ln = Ce, Dy, Ho) were used as the lanthanide oxides. These starting materials were weighed out in the appropriate ratio and well-mixed in an agate mortar. The mixtures were pressed into pellets and enclosed with platinum tubes, and then it was sealed in evacuated silica tubes. Then they were fired at 1250 °C for 12−204 h. The obtained phases were identified by powder X-ray diffraction (XRD) measurements. For compounds with Ln = Gd−Lu, impurity phases (for example, 6L-perovskite $Ba_3LnRu_2O_9$[11–17] or pyrochlore $Ln_2Ru_2O_7$[18]) were formed due to easy sublimation of Ba oxides and Ru oxides. To decrease such an impurity phase, the excess amount (~30%) of $BaRuO_3$[19] was added during sample preparation. Specimens for neutron diffraction (ND) measurements (8 g) were also prepared for Ln = Pr, Tb by the same procedures.

Structural Analysis. The powder XRD patterns of $Ba_4LnRu_3O_{12}$ samples were collected in the range $10° \le \theta \le 120°$ using a 2θ step size of 0.02° with a Rigaku MultiFlex diffractometer. For $Ba_4PrRu_3O_{12}$ and $Ba_4TbRu_3O_{12}$, the powder ND patterns were collected in the range $2° \le \theta \le 152°$ using 2θ step size of 0.1° with the wavelength of 1.8265 Å, at room temperature for $Ba_4PrRu_3O_{12}$ and at room temperature and low temperatures (2.5−30 K) for $Ba_4TbRu_3O_{12}$. The measurements were performed on the Kinken powder diffractometer for high-resolution measurements, HERMES, of the Institute for Materials Research (IMR), Tohoku University,[20] installed at the JRR-3 M Reactor in the Japan Atomic Energy Agency (JAEA), Tokai. Crystal and magnetic structures were determined by the Rietveld technique with the program RIETAN-2000.[21]

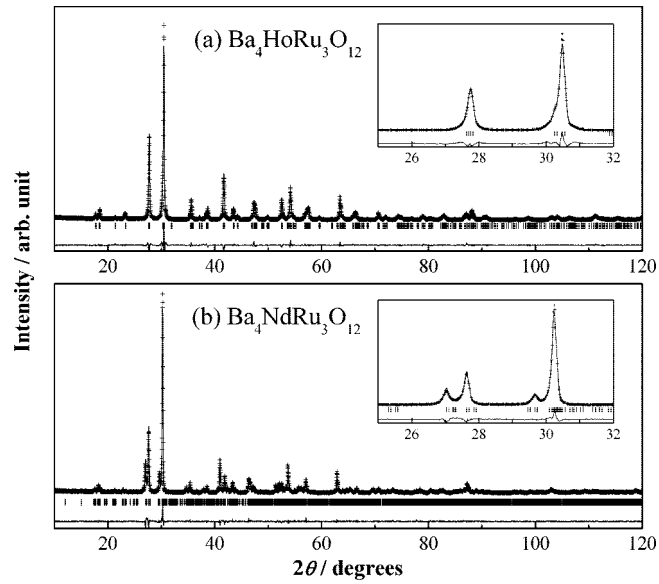

Figure 1. X-ray diffraction profiles for (a) $Ba_4HoRu_3O_{12}$ and (b) $Ba_4NdRu_3O_{12}$. The inset graphs show the profiles between $25° \le 2\theta \le 32°$.

Magnetic and Thermal Measurements. The magnetic measurements were carried out with a SQUID magnetometer (Quantum Design, MPMS-5S). The temperature dependence of the magnetic susceptibilities was measured under both zero-field-cooled (ZFC) and field-cooled (FC) conditions in an applied field of 0.1 T over the temperature range 1.8−400 K.

Specific heat measurements were performed by a relaxation technique with a heat capacity measurement system (Quantum Design, PPMS model) in the temperature range 1.8−300 K. The pelletized sample was mounted on a thin alumina plate with grease for better thermal contact.

Results and Discussion

Synthesis and Structural Analyses. We succeeded in synthesizing new perovskite-related compounds $Ba_4LnRu_3O_{12}$ (Ln = La−Nd, Sm−Lu). For some compounds, very small amounts (1−3%) of impurity phases still remained. They were 6L-perovskite $Ba_3LnRu_2O_9$[11–17] for compounds with Ln = La and Yb, and pyrochlore $Ln_2Ru_2O_7$[18] for compounds with Ln = Tb, Dy, Tm, and Lu.

The powder XRD patterns for $Ba_4HoRu_3O_{12}$ and $Ba_4NdRu_3O_{12}$ are shown in Figure 1. In the case of Ln = Tb−Lu, the diffraction peaks can be indexed with a hexagonal unit cell with the rhombohedral space group $R\bar{3}m$ (No.166), which are similar to those for the 12L-perovskites $Ba_4LnMn_3O_{12}$ (Ln = Ce, Pr)[22] and $Ba_4ZrRu_3O_{12}$.[23] Thus, the structural data for the $Ba_4LnMn_3O_{12}$ were used for the starting model of the present Rietveld analysis. The fitting results are shown in Figure 1a, and the good agreement between the observed and calculated intensities has been obtained. The determined crystal structure is illustrated in

(18) Taira, N.; Wakeshima, M.; Hinatsu, Y. *J. Phys.: Condens. Matter* **1999**, *11*, 6983–6990.
(19) Donohue, P. C.; Katz, L.; Ward, R. *Inorg. Chem.* **1965**, *4*, 306–310.
(20) Ohoyama, K.; Kanouchi, T.; Nemoto, K.; Ohashi, M.; Kajitani, T.; Yamaguchi, Y. *Jpn. J. Appl. Phys.* **1998**, *37*, 3319–3326.
(21) Izumi, F.; Ikeda, T. *Mater. Sci. Forum* **2000**, *321−324*, 198–203.
(22) Fuentes, A. F.; Boulahya, K.; Amador, U. *J. Solid State Chem.* **2004**, *177*, 714–720.
(23) De Vreugd, C. H.; Zandbergen, H. W.; IJdo, D. J. W. *Acta Crystallogr. C* **1984**, *40*, 1987–1989.

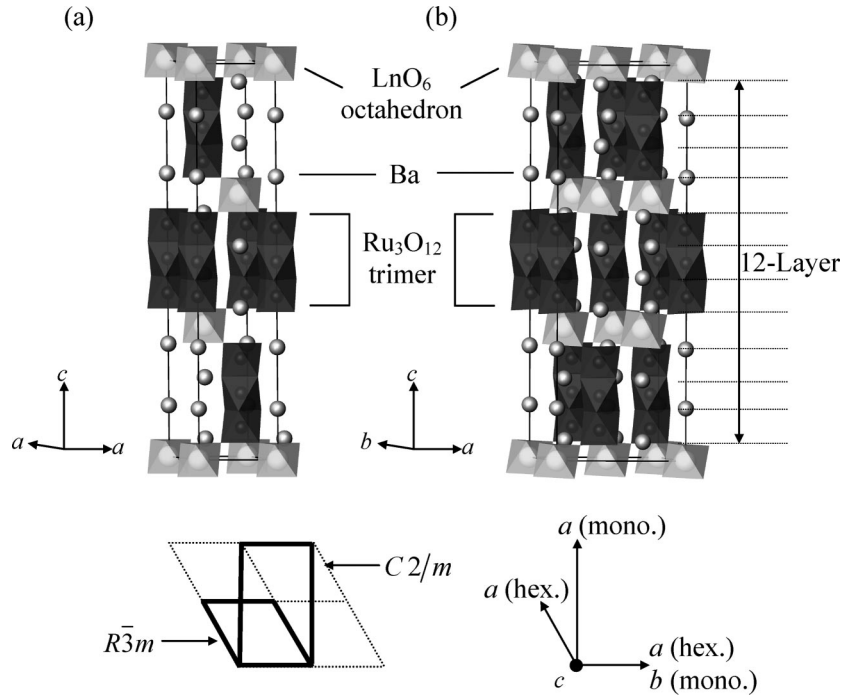

Figure 2. Crystal structure of $Ba_4LnRu_3O_{12}$. (a) and (b) show the hexagonal unit cell for Ln = Tb−Lu compounds and the monoclinic unit cell for Ln = La−Nd, Sm−Gd compounds, respectively.

Table 1. Structural Parameters for $Ba_4HoRu_3O_{12}$; Space Group $R\bar{3}m$ (No. 166), $z = 3$[a]

atom	site	*x*	*y*	*z*	*B*/Å^2
Ba(1)	6c	0	0	0.1291(1)	0.56(4)
Ba(2)	6c	0	0	0.2850(1)	0.97(6)
Ho	3a	0	0	0	0.14(7)
Ru(1)	3b	0	0	$^1/_2$	0.42(8)
Ru(2)	6c	0	0	0.4126(1)	0.70(7)
O(1)	18h	0.4905(8)	0.5095(8)	0.1230(3)	1.16(29)
O(2)	18h	0.4869(9)	0.5131(9)	0.2898(4)	1.16(27)

[a] $a = 5.8623(2)$ Å, $c = 29.0394(10)$ Å; $R_{wp} = 10.86\%$, $R_I = 2.62\%$, $R_e = 7.99\%$.

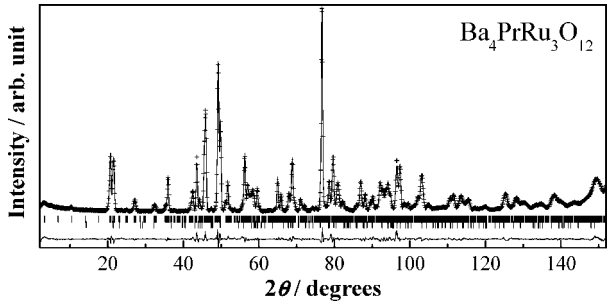

Figure 3. Powder neutron diffraction profiles for $Ba_4PrRu_3O_{12}$ at room temperature. The upper and bottom vertical marks represent the nuclear reflections for $Ba_4PrRu_3O_{12}$ and for the impurity $BaRuO_3$, respectively.

Figure 2a, and refined structural parameters for Ln = Ho compound are listed in Table 1.

On the other hand, some diffraction peaks for the compounds with Ln = La−Gd are significantly split as compared with those for Ln = Tb−Lu (see insets in Figure 1). This fact indicates that these compounds must have a lower symmetry than $R\bar{3}m$. To determine this crystal structure, powder ND measurements were carried out for $Ba_4PrRu_3O_{12}$ at room temperature (Figure 3). For the analysis of this data, we applied some subgroups of $R\bar{3}m$ and finally found that a monoclinic unit cell with space group $C2/m$ (No.12), $a_{mono} \sim \sqrt{3}a_{hex}$, $b_{mono} \sim a_{hex}$, $c_{mono} \sim c_{hex}$, and $\beta_{mono} \sim 90°$, gave a good fitting. The fitting results using this model are shown in Figure 3. The crystal structure determined is shown in Figure 2b, and obtained structural parameters and some selected bond lengths are summarized in Tables 2 and 3.

Table 2. Structural Parameters for $Ba_4PrRu_3O_{12}$; Space Group $C2/m$ (No. 12), $z = 6$[a]

atom	site	*x*	*y*	*z*	*B*/Å^{2b}
Ba(1)	4i	0.337(4)	0	0.537(1)	0.60(4)
Ba(2)	4i	0.336(5)	0	0.383(1)	0.60(4)
Ba(3)	4i	−0.002(4)	0	0.283(1)	0.60(4)
Ba(4)	4i	0.339(4)	0	0.795(1)	0.60(4)
Ba(5)	4i	0.000(4)	0	0.134(1)	0.60(4)
Ba(6)	4i	0.333(5)	0	0.951(1)	0.60(4)
Pr(1)	4i	0.339(5)	0	0.667(2)	0.57(12)
Pr(2)	2a	0	0	0	0.57(12)
Ru(1)	2c	0	0	$^1/_2$	0.51(4)
Ru(2)	4i	0.008(3)	0	0.415(1)	0.51(4)
Ru(3)	4i	0.326(3)	0	0.250(1)	0.51(4)
Ru(4)	4i	0.332(4)	0	0.165(1)	0.51(4)
Ru(5)	4i	0.332(3)	0	0.078(1)	0.51(4)
O(1)	4i	0.161(4)	0	0.460(1)	0.84(3)
O(2)	4i	0.148(4)	0	0.629(1)	0.84(3)
O(3)	4i	0.489(4)	0	0.291(1)	0.84(3)
O(4)	4i	0.821(4)	0	0.790(1)	0.84(3)
O(5)	4i	0.487(4)	0	0.127(1)	0.84(3)
O(6)	4i	0.818(5)	0	0.960(2)	0.84(3)
O(7)	8j	0.423(4)	0.730(5)	0.457(1)	0.84(3)
O(8)	8j	0.408(3)	0.726(5)	0.622(1)	0.84(3)
O(9)	8j	0.253(3)	0.749(4)	0.713(1)	0.84(3)
O(10)	8j	0.091(3)	0.735(4)	0.787(1)	0.84(3)
O(11)	8j	0.243(3)	0.729(4)	0.875(1)	0.84(3)
O(12)	8j	0.081(3)	0.734(5)	0.957(1)	0.84(3)

[a] $a = 10.157(7)$ Å, $b = 5.869(0)$ Å, $c = 29.315(1)$ Å, $\beta = 90.910(3)°$; $R_{wp} = 5.39\%$, $R_I = 0.93\%$, $R_e = 1.96\%$. [b] The temperature factors (*B*) were fixed on the same values for each element.

The crystal structure for the $Ba_4LnRu_3O_{12}$ compounds is described in the following. Three RuO_6 octahedra are connected to each other by face-sharing and form a Ru_3O_{12} trimer. The Ru_3O_{12} trimers and LnO_6 octahedra are alternately

Table 3. Selected Bond Lengths (Å) for $Ba_4PrRu_3O_{12}$ at Room Temperature

Ru(1)−O(7) ×4	2.00(3)	Pr(1)−O(2)	2.21(7)
Ru(1)−O(1) ×2	2.03(4)	Pr(1)−O(3)	2.13(7)
Ru(2)−O(1)	2.01(5)	Pr(1)−O(8) ×2	2.19(5)
Ru(2)−O(2)	2.03(5)	Pr(1)−O(9) ×2	2.19(5)
Ru(2)−O(7) ×2	2.02(4)	Pr(2)−O(6) ×2	2.18(4)
Ru(2)−O(8) ×2	1.93(3)	Pr(2)−O(12) ×4	2.18(3)
Ru(3)−O(3)	2.03(5)	**Pr−O (average)**	**2.18**(5)
Ru(3)−O(4)	1.89(5)		
Ru(3)−O(9) ×2	2.01(3)		
Ru(3)−O(10) ×2	1.96(4)	Ru(1)−Ru(2)	2.49(3)
Ru(4)−O(4)	2.05(6)	Ru(3)−Ru(4)	2.48(4)
Ru(4)−O(5)	1.95(5)	Ru(4)−Ru(5)	2.56(4)
Ru(4)−O(10) ×2	2.10(3)	**Ru−Ru (average)**	**2.51(4)**
Ru(4)−O(11) ×2	1.93(3)		
Ru(5)−O(5)	2.12(4)		
Ru(5)−O(6)	1.86(5)		
Ru(5)−O(11) ×2	2.09(4)		
Ru(5)−O(12) ×2	1.93(4)		
Ru−O (average)	**2.00(4)**		

linked by corner-sharing. As shown in Figure 2, perovskite-type structure with 12 layers are formed (the stacking sequence: *abcbcababcac*...).[10] In these structures, the distances between Ru atoms in the Ru_3O_{12} trimer are determined to be 2.48−2.60 Å, which are much shorter than double the metallic radius of Ru (2.68 Å).[24]This means that a strong magnetic interaction between Ru ions in the trimer should exist.

The variation of the average Ln−O bond length for $Ba_4LnRu_3O_{12}$ with the ionic radius of Ln^{3+} is plotted in Figure 4, which shows a monotonous increase except for Ln = Ce, Pr, and Tb. For these three compounds, the Ln−O lengths (2.21(14), 2.18(5), and 2.11(1) Å, respectively) are much shorter than those expected from this trend, and they are close to the values for Ln^{4+}−O^{2-} (2.27, 2.25, 2.16 Å) calculated from the Shannon's ionic radius[25] rather than those for Ln^{3+}−O^{2-} (2.41, 2.39, 2.32 Å). These facts strongly indicate that the Ln ions are in the tetravalent state. Similar results have been reported in the 6L-perovskites $Ba_3LnM_2O_9$ (M = Ru, Ir).[11–17,26,27] If there exist no oxygen defects, the oxidation state of Ln and Ru are both tetravalent for Ln = Ce, Pr, Tb compounds, and Ln ions are in the trivalent state and the oxidation state of Ru ions is +4.33 for other compounds.

Figure 5 shows the variation of lattice parameters with the ionic radius of Ln^{3+} in the six-coordination. Except for the compounds having the Ln^{4+} ion (Ln = Ce, Pr, and Tb), the lattice parameters, a_{hex} and c_{hex} (for the hexagonal cell)

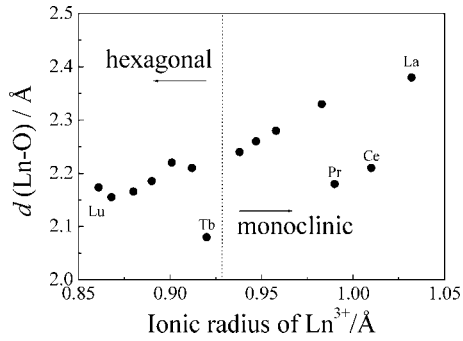

Figure 4. Variation of average Ln−O distances d(Ln−O) against the ionic radius of Ln^{3+}.

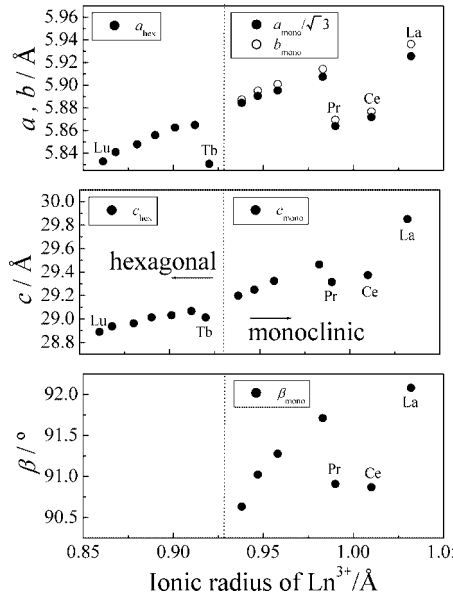

Figure 5. Variation of lattice parameters for $Ba_4LnRu_3O_{12}$ against the ionic radius of Ln^{3+}.

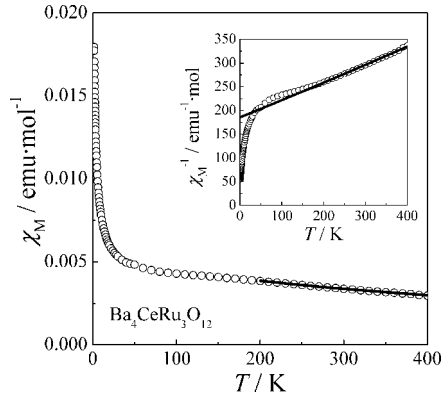

Figure 6. Temperature dependence of the magnetic susceptibilities for $Ba_4CeRu_3O_{12}$. The applied field is 0.1 T. The inset shows the reciprocal magnetic susceptibility. The solid line is the susceptibility calculated from the Curie−Weiss law.

and a_{mono}, b_{mono}, and c_{mono} (for the monoclinic cell), monotonously increase with the Ln^{3+} ionic radius. In the monoclinic region, the β_{mono} increases and the difference between $a_{mono}/\sqrt{3}$ and b_{mono} spreads with increasing the Ln^{3+} ionic radius. This fact indicates that the crystal structures of $Ba_4LnRu_3O_{12}$ are more distorted as the size of the Ln^{3+} ion becomes larger.

Magnetic Susceptibility and Specific Heat. The temperature dependencies of magnetic susceptibility and specific heat for $Ba_4CeRu_3O_{12}$ are plotted in Figures 6 and 7a, respectively. Both sets of data showed no magnetic anomaly down to 1.8 and 0.5 K, respectively. The magnetic property of $Ba_4CeRu_3O_{12}$ depends on only Ru^{4+} ions in the Ru_3O_{12} trimers because the Ce^{4+} ion is nonmagnetic. The magnetic susceptibility data above 200 K were fitted by the Curie−Weiss law, $\chi_M = C/(T - \theta) + \chi_{TIP}$, where C, θ, and χ_{TIP} mean the

(24) Wells, A. F. *Structural inorganic chemistry, 5th ed.*; Clarendon Press: Oxford, 1984.
(25) Shannon, R. D. *Acta Crystallogr. A* **1976**, *32*, 751–767.
(26) Doi, Y.; Hinatsu, Y. *J. Phys.: Condens. Matter* **2004**, *16*, 2849–2860.
(27) Lufaso, M. W.; Loye, H.-C. *Inorg. Chem.* **2005**, *44*, 9143–9153.

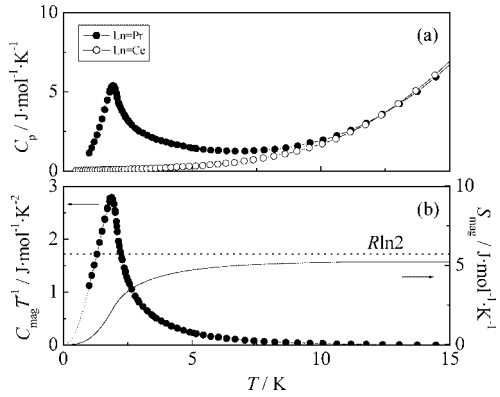

Figure 7. Temperature dependence of (a) the specific heat for $Ba_4CeRu_3O_{12}$ and $Ba_4PrRu_3O_{12}$ and (b) the magnetic specific heat and the magnetic entropy for $Ba_4PrRu_3O_{12}$. On (b), the magnetic specific heat data below 0.5 K were extrapolated from the relation of $C_{mag}/T \propto T^2$ (dotted line).

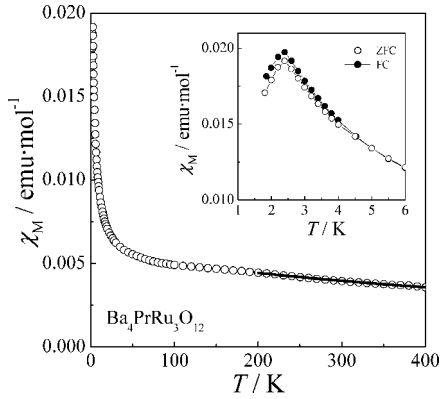

Figure 8. Temperature dependence of the magnetic susceptibilities for $Ba_4PrRu_3O_{12}$. The solid line is the susceptibility calculated from the Curie−Weiss law. The inset shows the magnetic susceptibilities at low temperatures.

Curie constant, Weiss constant, and temperature-independent paramagnetic susceptibility. The fitting curve is shown in the inset of Figure 6. The effective magnetic moment (μ_{eff}) and Weiss constant are determined to be 5.01(2) μ_B/mol (2.89 μ_B/Ru) and −550(8) K. The μ_{eff} agrees with the moment expected from the low-spin Ru^{4+} ion ($S = 1$; 2.83 μ_B/Ru). The large negative Weiss constant indicates the existence of the strong antiferromagnetic interaction between Ru ions in the Ru_3O_{12} trimer.

The temperature dependence of magnetic susceptibility for $Ba_4PrRu_3O_{12}$ is plotted in Figure 8. The Curie−Weiss fitting for the data above 200 K gives an effective magnetic moment of 5.85(3) μ_B/mol, which is close to the magnetic moment calculated from the free ion values:

$$\mu_{eff} = \sqrt{3 \times \mu_{Ru^{4+}}{}^2 + \mu_{Pr^{4+}}{}^2} = 5.52\ \mu_B/\text{mol}$$

The large negative Weiss constant −703(11) K also implies the strong antiferromagnetic interaction in the Ru_3O_{12} trimer.

At 2.4 K, it is found that this compound shows an antiferromagnetic anomaly (see inset in Figure 8). The specific heat (Figure 7a) also shows an anomaly at the same temperature. These experimental results indicate the occurrence of the long-range antiferromagnetic ordering. The magnetic specific heat (C_{mag}) and magnetic entropy (S_{mag}) were calculated from these data. In this calculation, we used

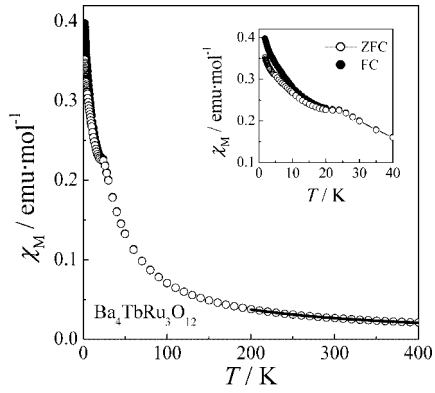

Figure 9. Temperature dependence of the magnetic susceptibilities for $Ba_4TbRu_3O_{12}$. The solid line is the susceptibility calculated from Curie−Weiss law. The inset shows the magnetic susceptibilities at low temperatures.

the data for $Ba_4CeRu_3O_{12}$ as the lattice contribution of the specific heat for $Ba_4PrRu_3O_{12}$, i.e., $C_{mag} = C_{Pr} - C_{Ce}$ and $S_{mag} = \int (C_{mag}/T)\, dT$; the result is plotted in Figure 7b. The magnetic entropy change due to the observed transition was 5.20 J/mol·K, which is close to R ln 2 = 5.76 J/mol·K. This fact indicates that the antiferromagnetic ordering is due to the ground Kramers doublet of Pr^{4+} in a low symmetric crystal field.

It is remarkable that the Ru_3O_{12} trimer in $Ba_4CeRu_3O_{12}$ does not show any long-range magnetic ordering (Figure 6 and 7a). Even when the strong antiferromagnetic interaction between Ru^{4+} ions exist, an uncancelled magnetic moment remains in the Ru_3O_{12} trimer, just like an up−down−up spin configuration. The absence of the long-range magnetic ordering may be due to the fact that the Ru_3O_{12} trimer in the $Ba_4CeRu_3O_{12}$ is isolated by the nonmagnetic CeO_6 octahedra, as shown in its crystal structure (Figure 2b).

On the other hand, the magnetic anomaly observed at 2.4 K in $Ba_4PrRu_3O_{12}$ (Figure 8) suggests the existence of long-range magnetic ordering. Since the magnetic interaction between 4f electrons is generally very weak, and since the distance between Pr ions is 5.87 Å in the $Ba_4PrRu_3O_{12}$, it is difficult to consider that only the magnetic moment of Pr ions are responsible for this magnetic interaction. The magnetic moment of the Ru_3O_{12} trimer should participate in the long-range magnetic ordering.

The temperature dependence of magnetic susceptibility for $Ba_4TbRu_3O_{12}$ is plotted in Figure 9. The Curie−Weiss fitting for the data above 200 K is also shown in this figure; the μ_{eff} and θ are 8.78(4) μ_B/mol and −57(3) K, respectively. The value of the μ_{eff} is much closer to 9.33 μ_B/mol (for Tb^{4+} + $3Ru^{4+}$) rather than 11.20 μ_B/mol (for Tb^{3+} + $2Ru^{4+}$ + Ru^{5+}).

The onset of the divergence between ZFC and FC susceptibilities indicates the occurrence of a magnetic transition at 24 K. The temperature dependence of the specific heat is plotted in Figure 10a. The data show two anomalies at 24 and 5 K. The specific anomaly at 24 K corresponds to the result by the magnetic susceptibility measurements, indicating the occurrence of the long-range antiferromagnetic ordering. The other broad peak observed at 5 K may be attributed to a feature of the ordering of the Tb^{4+} ion with large spin degeneracy ($2S + 1 = 8$). Most of

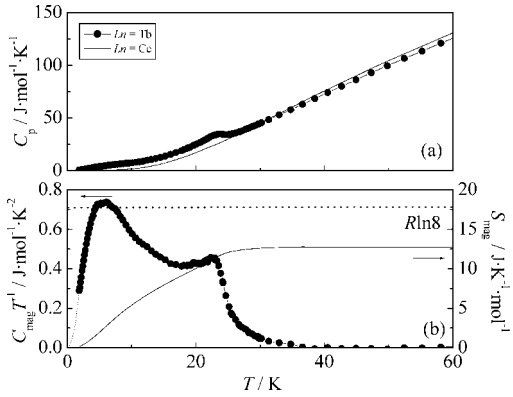

Figure 10. Temperature dependence of (a) the specific heat and (b) the magnetic specific heat and the magnetic entropy for $Ba_4TbRu_3O_{12}$. On (b), the magnetic specific heat data below 1.8 K were extrapolated from the relation of $C_{mag}/T \propto T^2$ (dotted line).

the magnetic entropy change often concentrates sufficiently below T_N in the case of compounds with $4f^7$ ions. This phenomenon has been demonstrated experimentally and theoretically in the references.[28–29]

The magnetic entropy was calculated by the same method as that for the $Ba_4PrRu_3O_{12}$ and it is shown in Figure 10b. The total magnetic entropy change is 12.5 J/mol·K, which is much smaller than that expected from R ln 8 = 17.3 J/mol·K for the Tb^{4+} ion. This discrepancy is due to the fact that the C_p of $Ba_4CeRu_3O_{12}$ is not appropriate for estimating the lattice contribution C_{lat} to the total specific heat for $Ba_4TbRu_3O_{12}$ because these two compounds have a different symmetry ($C2/m$ and $R\bar{3}m$), as described above. Another reason for this may be that the magnetic entropy is partially lost at higher temperatures because of the short-range ordering.

Neutron Diffraction Measurements for $Ba_4TbRu_3O_{12}$. Powder ND measurements for $Ba_4TbRu_3O_{12}$ were carried out at several temperatures to obtain further information about its structure and magnetic properties. Figure 11 shows the ND profiles collected at room temperature, 27 K, and 2.5 K. We succeeded in the Rietveld analysis for the data collected at room temperature by the application of the same structural model (space group $R\bar{3}m$). The crystal structure at low temperatures is the same as that at room temperature, i.e., the structural phase transition is not found in this compound. The structural parameters and some selected bond lengths are summarized in Tables 4 and 5, respectively. All the important bond lengths are not changed between the room temperature and 2.5 K.

Below 24 K, a number of low-angle peaks appeared, which are associated with the antiferromagnetic ordering. These reflections can be indexed using a propagation vector $\mathbf{k}$ = (0, 0, $^3/_2$). We have tested many models expected from the symmetry of the crystal structure and the propagation vector and finally found that a collinear antiferromagnetic structure model brought about a good calculation result. The calculated profile at 2.5 K is plotted in Figure 11c, and the magnetic

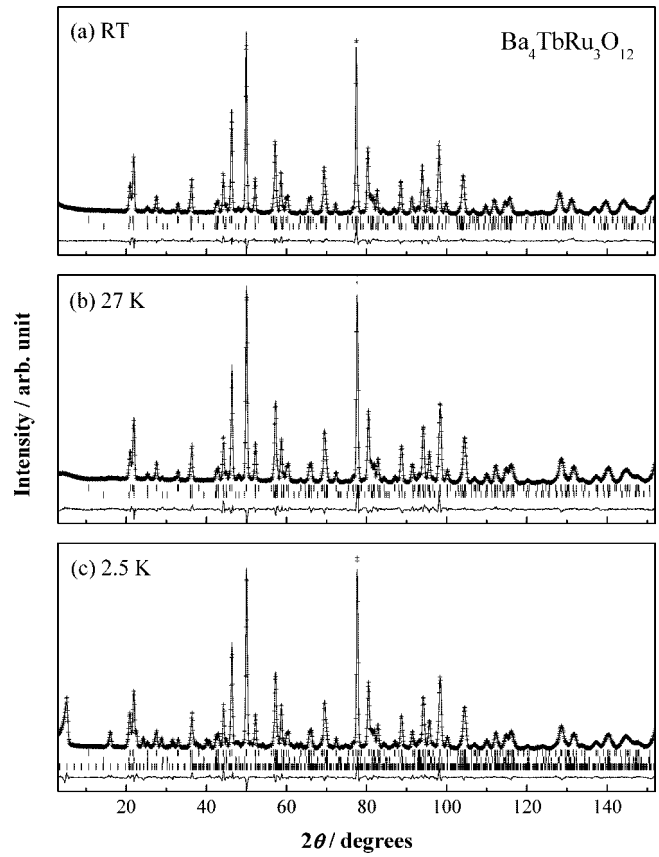

Figure 11. Powder neutron diffraction profiles for $Ba_4TbRu_3O_{12}$ at (a) room temperature, (b) 27 K, and (c) 2.5 K. On (a) and (b), the upper and bottom vertical marks represent the nuclear reflections for $Ba_4TbRu_3O_{12}$ and for the impurity $Ba_3TbRu_2O_9$, respectively. The bottom vertical marks on (c) represent the magnetic reflections for $Ba_4TbRu_3O_{12}$.

Table 4. Structural Parameters for $Ba_4TbRu_3O_{12}$; Space Group $R\bar{3}m$ (No. 166), z = 3

atom	site	x	y	z	B/Å^2
Room Temperature[a]					
Ba(1)	6c	0	0	0.1299(2)	0.80(7)
Ba(2)	6c	0	0	0.2850(1)	0.75(8)
Tb	3a	0	0	0	0.30(8)
Ru(1)	3b	0	0	$^1/_2$	0.53(7)
Ru(2)	6c	0	0	0.4133(1)	0.76(7)
O(1)	18h	0.4879(2)	0.5121(2)	0.1233(1)	0.84(4)
O(2)	18h	0.4955(2)	0.5045(2)	0.2914(1)	1.06(4)
27 K[b]					
Ba(1)	6c	0	0	0.1296(2)	0.48(8)
Ba(2)	6c	0	0	0.2861(2)	0.52(9)
Tb	3a	0	0	0	0.01(9)
Ru(1)	3b	0	0	$^1/_2$	0.36(7)
Ru(2)	6c	0	0	0.4132(1)	0.99(8)
O(1)	18h	0.4894(2)	0.5106(2)	0.1232(1)	0.60(5)
O(2)	18h	0.4956(3)	0.5044(3)	0.2911(1)	0.75(5)
2.5 K[c]					
Ba(1)	6c	0	0	0.1299(2)	0.35(8)
Ba(2)	6c	0	0	0.2859(2)	0.22(9)
Tb	3a	0	0	0	0.12(9)
Ru(1)	3b	0	0	$^1/_2$	0.15(7)
Ru(2)	6c	0	0	0.4131(1)	0.49(8)
O(1)	18h	0.4890(2)	0.5110(2)	0.1234(1)	0.52(5)
O(2)	18h	0.4952(3)	0.5048(3)	0.2911(1)	0.65(5)

[a] a = 5.8314(2) Å, c = 29.0212(8) Å; R_{wp} = 5.22%, R_I = 1.29%, R_e = 2.29%. [b] a = 5.8165(1) Å, c = 28.9731(9) Å; R_{wp} = 6.25%, R_I = 1.71%, R_e = 2.80%. [c] a = 5.8144(2) Å, c = 28.9648(0) Å, M_{Ru} = 0.96(11) μ_B, M_{Tb} = 5.78(7) μ_B; R_{wp} = 6.52%, R_I = 1.29%, R_e = 2.59%.

structure is illustrated in Figure 12. In this magnetic structure, the magnetic moments of Tb and Ru ions are collinear and lie on the *ab* plane. The exact direction in the *ab* plane could not be determined. The Ru moments in the Ru_3O_{12} trimer

(28) Bouvier, M.; Lethuillier, P.; Schmitt, D. *Phys. Rev. B* **1991**, *43*, 13137–13144.
(29) Blanco, J. A.; Gignoux, D.; Schmitt, D. *Phys. Rev. B* **1991**, *43*, 13145–13151.

Table 5. Selected Bond Lengths (Å) for $Ba_4TbRu_3O_{12}$

	RT	27 K	2.5 K
Tb−O(2) ×6	2.114(2)	2.113(2)	2.117(3)
Ru(1)−O(1) ×6	2.006(2)	2.014(2)	2.008(2)
Ru(2)−O(1) ×3	2.003(3)	2.012(4)	2.012(4)
Ru(2)−O(2) ×3	1.976(3)	1.966(3)	1.959(3)
Ru−O (average)	**1.997(3)**	**2.002(3)**	**1.997(3)**
Ru(1)−Ru(2)	2.515(3)	2.513(8)	2.516(7)

order ferrimagnetically. Along the *c* axis, each of the magnetic moments for Tb and Ru ions are alternately stacked. The temperature dependence of ordered magnetic moments for Tb and Ru ions is plotted in Figure 13. The magnetic moment of Tb gradually increases with decreasing temperature and reaches 5.7 μ_B at 2.5 K, and the Ru moment is almost saturated (∼1 μ_B/Ru). Both the moments begin to align almost at the same temperature; thus, this antiferromagnetic transition should be due to their cooperative ordering. This result is contrastive with the cases for the 6L-perovskite $Ba_3TbRu_2O_9$, where no evidence of the long-range magnetic ordering of Ru^{4+} ions was found.[15] This difference may be due to the relatively strong magnetic interaction between Tb^{4+} ions and Ru_3O_{12} trimer via the Tb−O−Ru pathway owing to an uncancelled magnetic moment in the Ru_3O_{12} trimer .

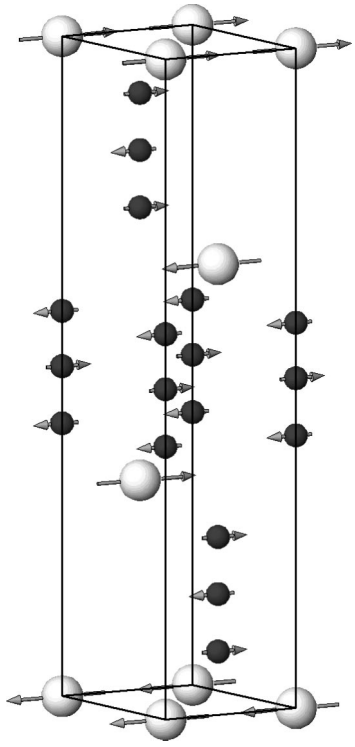

Figure 12. One-half of the magnetic structure for $Ba_4TbRu_3O_{12}$ at 2.5 K.

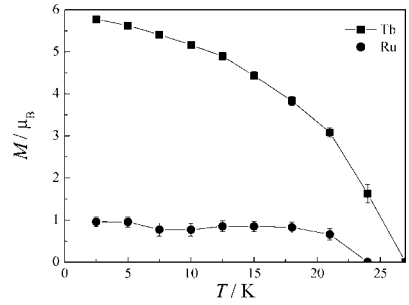

Figure 13. Temperature dependence of the magnetic moments of Tb^{4+} and Ru^{4+} for $Ba_4TbRu_3O_{12}$.

Summary

New oxides $Ba_4LnRu_3O_{12}$ (Ln = lanthanides) have been successfully synthesized. They are crystallized in the 12L-perovskite-type structures consisting of Ru_3O_{12} trimers and LnO_6 octahedra. In the cases of Ln =La−Nd, Sm−Gd, they adopt the monoclinic structure, and Ln = Tb−Lu have the hexagonal structure.

While no magnetic anomaly was observed down to 0.5 K for $Ba_4CeRu_3O_{12}$, $Ba_4PrRu_3O_{12}$ showed an antiferromagnetic transition at 2.4 K, which should be ascribable to the magnetic Pr^{4+} ions. $Ba_4TbRu_3O_{12}$ showed an antiferromagnetic transition at 24 K. In the ND measurements at 2.5 K, both Tb^{4+} and Ru^{4+} ions showed long-range magnetic ordering.

Acknowledgment. This work was supported by a Grant-in-aid for Scientific Research of Priority Area "Panoscopic Assembling and High Ordered Functions for Rare Earth Materials" No. 19018003 from the Ministry of Education, Science, Sports, and Culture of Japan.

CM800708G